Tau neutrino

Adriano Cherchiglia,[1] O. L. G. Peres,[1] and E. S. Souza[1]

[1]*Instituto de Física Gleb Wataghin - UNICAMP, 13083-859, Campinas SP, Brazil*

AAAAAAAAAAA

I. INTRODUCTION

** **Ed** **: We explore the capabilities of the upcoming Deep Underground Neutrino Experiment (DUNE) to measure ν_τ charged-current interactions and the associated oscillation probability $P(\nu_\mu \to \nu_\tau)$ at its far and near detector, concentrating on how such results can be used to probe neutrino properties and interactions included NSI. DUNE has the potential to identify significantly more ν_τ events than all existing experiments and can use this data sample to nontrivially test the three-massive-neutrinos paradigm by providing complementary measurements to those from the ν_e appearance and ν_μ disappearance channels. Throughout, we also consider the relative benefits of the proposed high-energy tune of the Long-Baseline Neutrino Facility (LBNF) beam-line.

** **Ed** **: Over the last twenty years, our understanding of neutrino-flavor change as a function of the neutrino proper time has improved exponentially. The old solar and atmospheric neutrino anomalies evolved into the very robust three-massive-neutrinos paradigm, which postulates that neutrinos, while still interacting with ordinary matter as prescribed by the standard model of particle physics (SM), have distinct, non-zero masses and that the neutrino flavor-eigenstates ν_α, $\alpha = e, \mu, \tau$, are non-trivial linear superpositions of the neutrino mass-eigenstates ν_i, with masses m_i, $i = 1, 2, 3$: $\nu_\alpha = U_{\alpha i}\nu_i$, where $U_{\alpha i}$ are the coefficients of the 3×3 unitary lepton mixing matrix U.

** **Ed** **: Assuming the three-massive-neutrinos paradigm is correct, the oscillation parameters – those that determine U, along with the neutrino mass-squared differences $\Delta m^2_{ij} \equiv m^2_i - m^2_j$, $i, j = 1, 2, 3$ – are well constrained by existing neutrino data, with a few exceptions, including the neutrino mass ordering (or the sign of Δm^2_{31}) and the strength of leptonic CP-invariance violation. When it comes to both confirming the three-massive-neutrinos paradigm and determining the oscillation parameters, all current statistical power comes from studies of ν_μ and ν_e (plus antineutrinos) disappearance and $\nu_\mu \to \nu_e$ (plus antineutrinos) appearance. While there is definitive evidence for $\nu_\mu \to \nu_\tau$ appearance from both atmospheric [**? ? ?**] and beam [**?**] neutrino experiments, the quantitative impact of the current ν_τ appearance data is, at best, sub-dominant.

** **Ed** **: **********

Among the goals of the next-generation long-baseline neutrino experiments – the Long-Baseline Neutrino facility to the Deep Underground Neutrino Experiment (LBNF-DUNE) in the United States and the Tokai to Hyper-Kamiokande (T2HK) experiment in Japan – are the precision measurements of neutrino oscillation parameters, exploring CP-invariance violation in the neutrino sector, and, perhaps most important, testing the validity of the three-massive-neutrinos paradigm and looking for more new physics in the neutrino sector. There are several studies in the literature, including those pursued by the collaborations, of the physics reach of LBNF-DUNE and T2HK, including their sensitivities to a variety of hypothetical new neutrino physics scenarios. All of these explore the ν_μ disappearance and the $\nu_\mu \to \nu_e$ appearance (plus antineutrinos) channels.

** **Ed** **: **********

Here, instead, we explore the physics reach of the beam ν_τ appearance data that is accessible to LBNF-DUNE. Direct measurements of ν_τ appearance, both in atmospheric and beam neutrino experiments, are very challenging, for a variety of reasons. All neutrino experiments are of the fixed-target type and the large τ mass translates into relatively large thresholds for charged-current ν_τ scattering off of ordinary matter ($E_{\nu_\tau} \gtrsim 3.35$ GeV for $\nu_\tau + N \to \tau + N$, where N is a nucleon, and $E_{\nu_\tau} \gtrsim 3.1$ TeV for $\nu_\tau + e \to \tau + \nu_e$). Given the beam energies of LBNF-DUNE and T2HK, driven by the requirement that large Δm^2_{31}-driven oscillation effects are observed in the far detector, only LBNF-DUNE is expected to observe beam events with neutrino energies above the τ-threshold. Even at LBNF-DUNE, phase-space-suppression effects are large and the ν_τ appearance event sample is expected to contain, for the lifetime of the experiment, between 100 and 1,000 events. Identifying and reconstructing τ-leptons in neutrino detectors is also very challenging. The tracking resolution of liquid argon detectors, around several millimeters, is such that τ-leptons decay promptly and hence must be identified via their decay products. Furthermore, all τ leptons decay channels involve missing energy – $\tau \to \nu_\tau +$ something else. These imply that the ν_τ appearance channel is "dirty" and that the reconstruction of the ν_τ energy is a larger challenge than that of the ν_μ and ν_e energies. We discuss our simulations of the ν_τ sample at LBNF-DUNE in Sec. **??**, including background estimates and the challenges of neutrino-energy reconstruction.

** **Ed** **: **********

The collection of a ν_τ-enriched sample is a nontrivial task. The high τ-production threshold, a consequence of the heavy τ-lepton mass, implies relatively very small statistics, and the fact that the τ leptons decay promptly and only semi-visibly implies that reconstructing the ν_τ energy is difficult and that the rejection of neutral-current backgrounds is challenging. These challenges are reflected in the results presented here. The sensitivity of the ν_τ-appearance channel, whenever comparisons are meaningful, is markedly inferior to that of the ν_e-appearance or the ν_μ-disappearance ones as one can readily confirm in Figs. **??** or **??**. On the other hand, we emphasize the complementarity of the different oscillation channels. Different hypotheses about the physics responsible for neutrino oscillations, including the very successful three-massive-neutrinos paradigm,

imply different correlations among oscillation channels and, in many cases, the ν_τ-appearance channel provides information that cannot be accessed in other ways.

**** Ed ****: ************************

In spite of all the challenges, LBNF-DUNE is expected to collect an unprecedented number of reconstructed beam ν_τ events. Here, we proceed to understand what nontrivial particle physics information one should be able to extract. We explore, assuming the three-massive-neutrinos paradigm, how well one can measure the ν_τ charged-current scattering cross section, and, assuming the standard model expectation for the ν_τ charged-current scattering cross section, how well the ν_τ appearance data can constrain oscillation parameters. As far as the latter exercise is concerned, we compare, in different ways, the sensitivity of the ν_τ appearance sample with that of the ν_e appearance and ν_μ disappearance samples. These results are presented and discussed in detail in Sec. **??**.

**** Ed ****: The production of τ leptons by charged-current ν_τ–nucleus scattering requires neutrino energies $E_\nu \gtrsim 3.4$ GeV. Furthermore, the prompt decay of the τ combined with the fact that all τ decays contain ν_τ in the final state prove a challenge for both identifying a scattering event as a ν_τ charged-current interaction and reconstructing the initial neutrino energy. Nonetheless, the LBNF beam will have a significant portion of its flux above the τ production energy threshold and liquid argon detectors are excellent at reconstructing final-state particles, allowing for at least a modest but unique ν_τ data sample. Here, we discuss our expectations regarding the capability of DUNE to identify ν_τ interactions and measure their energies.

**** Ed ****: NSI no meio dificilmente pode ser notado no DUNE, visto que o efeito de matéria é sub-dominante. Assim uma forma medir NSI usando o DUNE seria na produção.

II. EFT DESCRIPTION FOR CC NSI

It is customary to parametrize new effects due to the interaction of neutrinos with a medium as non-standard interactions (NSI). In this work we adopt a more general approach, considering NSI to denote not only BSM effects (new interactions) at neutrino propagation, but also at its production or detection. In order to make this distinction clearer, we notice that NSI connected with production are connected with charged-current (CC) processes (for the experiments to be analised in this work, the pion decay), while NSI connected with propagation are related to neutral currents (NC) processes. Restricting our attention to CC-NSI, they can be conveniently expressed by the EFT Lagrangian below [1, 2]

$$\begin{aligned}\mathscr{L}_{\rm WEFT} \supset -\frac{2\,V_{jk}^{CKM}}{v^2}\Big\{&[1+\epsilon_L^{jk}]_{\alpha\beta}\left(\bar{u}^j\gamma^\mu P_L d^k\right)\left(\bar{\ell}_\alpha\gamma_\mu P_L\nu_\beta\right)+[\epsilon_R^{jk}]_{\alpha\beta}\left(\bar{u}^j\gamma^\mu P_R d^k\right)\left(\bar{\ell}_\alpha\gamma_\mu P_L\nu_\beta\right)\\ &+\frac{1}{2}\left[\epsilon_S^{jk}\right]_{\alpha\beta}\left(\bar{u}^j d^k\right)\left(\bar{\ell}_\alpha P_L\nu_\beta\right)-\frac{1}{2}\left[\epsilon_P^{jk}\right]_{\alpha\beta}\left(\bar{u}^j\gamma^5 d^k\right)\left(\bar{\ell}_\alpha P_L\nu_\beta\right)\\ &+\frac{1}{4}\left[\epsilon_T^{jk}\right]_{\alpha\beta}\left(\bar{u}^j\sigma^{\mu\nu}P_L d^k\right)\left(\bar{\ell}_\alpha\sigma_{\mu\nu}P_L\nu_\beta\right)+\text{h.c.}\Big\}\,.\end{aligned} \tag{1}$$

Here, V^{CKM} is the Cabibbo-Kobayashi-Maskawa (CKM) matrix, $v = 1/(\sqrt{2}G_F) \approx 246\,\text{GeV}$ is the vacuum expectation value of the SM Higgs field and ϵ_X are the Wilson coeficients, with $X = L, R, S, P, T$ for left-handed, right-handed, scalar, pseudo-scalar and tensor, respectively. The Roman (Greek) symbols denote the quark (lepton) generations. This Lagrangian is based on the Weak Effective Field Theory (WEFT), defined below the electroweak scale.

In this work, we will be concerned only with CC NSI related to pion decay, therefore we only consider the case $j = k = 1$, and, for simplicity, drop the overscript on the WC hereafter. Moreover, it was shown (for instance in [1]) that only the WCs $\epsilon_{L,R,P}$ can affect pion decay. Since the pseudoscalar coefficient involves a chirality flipping (while the standard vertex, with the W-boson is chirality conserving), the WC ϵ_P will appear multiplied by a ratio of the pion mass over the mass of its constituents as well as the emitted charged lepton. Therefore, we will be able to constraint ϵ_P much more than $\epsilon_{L,R}$, motivating us to only consider ϵ_P to be non-null. Moreover, for simplicity, we denote hereafter $(\epsilon_P)_{\alpha\beta}$ as $\epsilon_{\alpha\beta}$.

Adopting a QFT description for neutrino oscillation, the differential event rate for neutrinos of flavor β with energy E_ν to be detected at a distance L from the source S, where they were produced with flavor α, is given by [3]

$$R^S_{\alpha\beta} = N_T\sigma^{\rm SM}_\beta(E_\nu)\Phi^{\rm SM}_\alpha(E_\nu)\sum_{k,l} e^{-i\frac{L\Delta m^2_{kl}}{2E_\nu}}\frac{[\mathscr{P}U]_{\alpha l}[U^\dagger\mathscr{P}^\dagger]_{k\alpha}}{[\mathscr{P}\mathscr{P}^\dagger]_{\alpha\alpha}}U_{\beta k}U^*_{\beta l}\,, \tag{2}$$

where $\Phi_\alpha^{\rm SM}$ is the SM flux, $\sigma_\beta^{\rm SM}$ is the SM cross-section, U is the PMNS matrix, and $\mathscr{P}$ is due to the CC NSI being given by

$$[\mathscr{P}]_{\alpha\beta} \equiv \delta_{\alpha\beta} - \frac{m_{\pi^\pm}^2}{m_{\ell_\alpha}(m_u + m_d)}\epsilon_{\alpha\beta}\,. \tag{3}$$

The denominator in eq.(2) is due to indirect effects, first introduced in [3]. It appears by writing the event rate in terms of the measured pion decay (thus defining $\Phi_\alpha^{\rm SM}$), which is a inclusive measurement regarding the emitted neutrino. As discussed in [**?**], if only diagonal CC NSI are considered, due to the indirect effects they will cancel in event rate. This is the case if a UV completion for the CC NSI comes only from BSM particles with masses above the electroweak scale. In the present work, we will not delve into UV completions. However, since we will consider only non-diagonal CC NSI (to be more precise, $\epsilon_{\mu\tau}$), the UV completion will typically require the inclusion of extra symmetries than the SM gauge group and the presence of BSM particles with masses below the electroweak scale.

III. TAU NEUTRINO SAMPLE AT DUNE

explain the approach, both for far and near detector
colocar grafico de eventos para espilons diferente de zero, ilustrando o efeito

** **Ed** **: We assume that the DUNE far detector, 1300 km from the neutrino source at Fermilab, consists of 40 kton of liquid argon (fiducial mass) and that the LBNF beam will deliver 1.1×10^{21} protons on target (POT) per year. We consider the currently-under-consideration tau-optimized flux [**?**] ("high-energy mode") – forward horn current (which we will refer to as "neutrino mode"), reverse horn current ("antineutrino mode"). The high-energy mode contains significantly higher-energy neutrinos than the other two modes, with a large fraction of the neutrinos above the τ threshold. For neutrino and antineutrino modes, we simulate event yields using the "CP-optimized fluxes" from Refs. [**? ?**]. In our analyses we consider two different hypotheses for DUNE's data-collection strategy. We perform analyses combining $3 + 3$ years of neutrino and antineutrino mode with an additional year of data taking in the high-energy mode, totaling seven years until the end of the DUNE experiment. We refer to this collection strategies as "$3 + 3 + 1$".

** **Ed** **: When a ν_τ interacts via a charged-current interaction, producing a τ lepton, the decay length of the τ is significantly smaller than the resolution of the DUNE detector, meaning that one must reconstruct the τ decay products in order to classify the incoming neutrino as a ν_τ. The authors of Ref. [**?**] investigated the capability of liquid argon detectors to identify ν_τ events using hadronic τ decays, which also make up the largest branching fraction for the τ (around 65% [**?**]). This approach takes advantage of the detector's capability to identify pions and kaons and to measure their kinematic properties. Understanding the usefulness of the leptonic τ decays, which are, naively, heavily contaminated by charged-current ν_μ or ν_e scattering, is beyond the scope of this manuscript. Building on Ref. [**?**], efforts within the DUNE collaboration [**?**] have optimistically estimated that one can isolate a ν_τ-rich event sample where 30% of hadronically-decaying τ events are successfully identified while only 0.5% of neutral-current background events remain. More sophisticated analyses are currently under intense investigation by the collaboration. We restrict ourselves to this rather optimistic scenario throughout this work, and hope that the results discussed here will help motivate more detailed studies of the ν_τ-reconstruction capabilities of DUNE and other liquid argon detectors.

** **Ed** **: When performing an oscillation analysis, it is paramount to measure the energy of the incoming neutrino. This is relatively straightforward[1] for charged-current events induced by ν_e and ν_μ, where the outgoing charged lepton is well-reconstructed. However, τ leptons are impossible to reconstruct perfectly, as their decays necessarily involve at least one outgoing neutrino. We have constructed a migration matrix mapping the true neutrino energy $E_\nu^{\rm true}$ to the reconstructed neutrino energy $E_\nu^{\rm reco}$, parameterizing it with a bias in the preferred reconstructed energy as a function of the true energy, as well as an uncertainty on the reconstructed energy. This is done by simulating final-state hadronic τ-decays using MADGRAPH [**?**] for different τ energies and computing the assumed-to-be observed energy in the hadronic system. Our simulations are consistent with the following simple picture. For a given $E_\nu^{\rm true}$, the reconstructed energy follows a Gaussian distribution with a mean value $bE_\nu^{\rm true}$ and width $\sigma_E = rE_\nu^{\rm true}$, where b is the bias and r is the resolution of the measurement. Our simulations point to $b \approx 45\%$ and $r \approx 25\%$. While the bias does not have a significant impact on the quantitative results presented in the following section, the resolution does; more detailed studies indicate that the DUNE collaboration will be able to achieve $8\% \lesssim r \lesssim 25\%$, and we choose the conservative upper limit [**?**]. Fig. 1 depicts the migration matrix we have obtained and

[1] Albeit not at all trivial and still under intense investigation, see, for example, Refs. [**? ?**].

will use for all forthcoming analyses. We have also performed a more realistic simulation using the GENIE3.0 software [**?**], and the results we obtained agree with Fig. 1.

FIG. 1. Migration matrix for hadronically-decaying τ leptons produced via ν_τ charged-current interactions. The assumed bias is 45% and the resolution is 25%, see text for details. No migration exists below $E_\nu^{\rm true} \approx 3.4$ GeV, below which the scattering process is kinematically forbidden.

**** Ed ****: ************************

Virtually no ν_τ are produced at the neutrino source. In the DUNE detector, however, the three-massive-neutrinos paradigm predicts a healthy ν_τ flux, mostly from $\nu_\mu \to \nu_\tau$ oscillations over the 1300 km baseline. Assuming the three-massive-neutrinos paradigm, the SM ν_τ scattering cross section, and incorporating the expected identification capability for hadronic τ events, we calculate the expected number of reconstructed events as a function of neutrino energy for each mode of beam operation. Fig. 8 depicts the expected number of signal events for the neutrino mode (left), the antineutrino mode (center), and the high-energy mode (right). Here, we assumed the following values for the oscillation parameters [**?**], in agreement with the most recent global-fit results obtained by the NuFit collaboration [**?**]:

$$\sin^2\theta_{12} = 0.310, \quad \sin^2\theta_{13} = 0.02240, \quad \sin^2\theta_{23} = 0.582, \quad \delta_{CP} = 217^\circ = -2.50\ \text{rad},$$
$$\Delta m^2_{21} = 7.39 \times 10^{-5}\ \text{eV}^2, \quad \Delta m^2_{31} = +2.525 \times 10^{-3}\ \text{eV}^2. \tag{4}$$

Unless otherwise stated, we will assume these oscillation parameters to be the true values in our analyses going forward. We discuss the details on the $\nu_\mu \to \nu_\tau$ oscillation probability in the next section. Fig. 8 depicts both "smeared" (solid histograms) and "unsmeared" (dashed histograms) event yields using the energy migration matrix discussed above. We divide the simulated data in energy bins of constant width $\Delta E_\nu = 0.5$ GeV, between 0 and 20 GeV, for our analyses.

FIG. 2. Expected number of ν_τ-identified signal events per 0.5 GeV bin as a function of the true (dashed) or reconstructed (solid) neutrino energy. The left panel displays the expected number of events when in neutrino mode, the center panel displays the antineutrino mode, and the right panel displays high-energy mode events. In each panel, we show the contribution due to neutrinos in green and antineutrinos in orange. Each distribution has been normalized to the expected runtime in each mode, 3.5 years for neutrino and antineutrino modes and 1 year for high-energy mode.

**** Ed ****: ****************************

Fig. 3 depicts the expected event yields – stacked – taking neutral-current backgrounds into account, along with the energy smearing. In seven years of running, we anticipate a healthy, relatively clean ν_τ-appearance sample. In the $3.5 + 3.5$ case, the sample includes over 200 events, while in the $3 + 3 + 1$ running scheme we expect over 300 events. In both cases, neutral-current backgrounds make up less than 50% of all events [**?**].

FIG. 3. Expected number of reconstructed ν_τ events per 0.5 GeV bin as a function of reconstructed energy. The left panel displays the expected number of events when in neutrino mode, the center panel displays the antineutrino mode, and the right panel displays high-energy mode events. We display stacked histograms of background (grey), events from $\overline{\nu}_\tau$ producing τ^+ leptons (orange), and events from ν_τ producing τ^- (green). Each distribution has been normalized to the expected runtime in each mode, 3.5 years for neutrino and antineutrino modes and 1 year for high-energy mode.

**** Ed ****: In our analyses, we include a 25% normalization uncertainty on the number of signal events, a conservative assumption related to systematic uncertainties regarding the neutrino flux, cross section, etc. We find, in practice, that this uncertainty does not have a strong impact on the results discussed in the next section.

**** Ed ****: We do not advocate for or favor any particular hypothesis for the physics that may exist beyond the three-massive-neutrinos paradigm. Instead, these are to be viewed as different, quantifiable modifications to the neutrino oscillation probabilities that serve as proxies for what may ultimately turn out to be the new physics. All hypotheses have been heavily scrutinized in the past so it is easy to make comparisons between different neutrino oscillation experiments and different oscillation channels.

**** Ed ****: Assuming the three-massive-neutrinos paradigm, in vacuum, for the LBNF-DUNE baseline $L = 1300$ km and neutrino energies above τ threshold ($E_\nu \gtrsim 3.4$ GeV),

$$P(\nu_\mu \to \nu_\tau) = 4|U_{\mu 3}|^2|U_{\tau 3}|^2 \sin^2\left(\frac{\Delta m^2_{31}L}{4E_\nu}\right) + \text{subleading}. \tag{5}$$

Numerically

$$\frac{\Delta m^2_{31}L}{4E_\nu} = 0.75\left(\frac{\pi}{2}\right)\times\left(\frac{3.5\text{GeV}}{E_\nu}\right)\left(\frac{\Delta m^2_{31}}{2.5\times 10^{-3}\text{ eV}^2}\right)\left(\frac{L}{1300\text{ km}}\right), \tag{6}$$

such that all reconstructed ν_τ appearance events occur above the first oscillation maximum. The oscillation amplitude is $4|U_{\tau 3}|^2|U_{\mu 3}|^2 = \cos^4\theta_{13}\sin^2 2\theta_{23} \sim 0.95$, using the NuFit results listed in Eqs. (4). The subleading terms include the "solar" oscillations and the interference term. Here, the subleading terms are indeed subleading: $\Delta m^2_{21}/\Delta m^2_{31} \sim 0.03$ and, unlike the case of $\nu_\mu \to \nu_e$ oscillations, all relevant elements of the lepton mixing matrix are large.[2] More quantitatively, for the energies of interest, we expect the interference term to be around a few percent of the leading term while the solar term is at the per-mille level. Matter effects, which we include in all numerical computations, are small and do not modify this picture. We provide more details in Appendix **??**.

**** Ed ****: Under these circumstances, it is virtually impossible, using $\nu_\mu \to \nu_\tau$, to determine the octant of θ_{23} (whether $\theta_{23} < \pi/4$ or $\theta_{23} > \pi/4$), since $P(\nu_\mu \to \nu_\tau)$ is, at leading order, invariant upon $|U_{\mu 3}|^2 \leftrightarrow |U_{\tau 3}|^2$. The same is true for the neutrino mass ordering since resolving the neutrino mass ordering with neutrino oscillations requires visible matter effects or the ability to resolve more than one mass-squared difference.

**** Ed ****: Fig. 4 depicts the $\nu_\mu \to \nu_\tau$ oscillation probability. All oscillation parameters are fixed to the values listed in Eqs. (4), except for $\sin^2\theta_{23}$. The shaded region corresponds to $\sin^2 2\theta_{\mu\tau} \in [0.5, 1]$.

FIG. 4. The oscillation probability $P(\nu_\mu \to \nu_\tau)$ as a function of neutrino energy E_ν. The blue-shaded region corresponds to neutrino energies below the τ production threshold. The grey band is spanned by allowing values of $\sin^2 2\theta_{\mu\tau} \in [0.5, 1]$. All other oscillation parameters are fixed to the values listed in Eqs. (4).

**** Ed ****: OBSERVATION: We do not depict two-dimensional projections of the parameter space that include the δ_{CP}-direction since the ν_τ-appearance channel is virtually insensitive to δ_{CP} (pois o efeito de matéria é sob-dominante. Contudo, com NSI-production poderiamos ver algo?).

****

Beginning to write

****

[2] In the case of $\nu_\mu \to \nu_e$ oscillations, the leading term is proportional to $|U_{e3}|^2 \sim 0.022 \ll 1$. In this case, the interference term can be almost as large as the leading term for LBNF-DUNE neutrino energies and baseline.

The Long-Baseline Neutrino Facility to Deep Underground Neutrino Experiment (LBNF-DUNE) is one of the next-generation oscillation neutrino experiments of long baseline, where we expect to extract more accurate data than in the current experiments. The next-generation experiments will not only provide an opportunity to test paradigms concerning oscillation neutrinos, such as three-mass neutrinos, but will also allow for more precise measurements of oscillation parameters. In addition, new physics can be investigated, such as non-standard interaction (NSI).

Falar mais Sobre novas gerações de detectores e NSI.

As discussed and simulated in the article [4], the DUNE experiment is expected to be one of the best known experiment capable of detecting ν_τ events. Especially when we consider τ-optimized fluxes,

The DUNE experiment is configured to take three years in both neutrinos mode (forward horn current) and antineutrinos mode (reverse horn current), plus one year of high-energy mode (forward horn current). Simulating a full seven-year analysis, indicated as $3 + 3 + 1$. The DUNE experiment is an appropriate alternative for studying new physics involving ν_τ oscillation. Since the statistic involving ν_τ is naturally low, any change is significantly meaningful, creating an incentive to search more detailed. In this section, we discuss the description math necessary to modify the ν_τ appearance events simulated in the article [4] by incorporating the NSI in the pion decay.

The DUNE experiment will use Fermilab's LBNF facilities for LBNF near site and also LBNF far site, with two detectors positioned at each site. Both detectors will make use of the new argon liquid technique to detect neutrinos. The LBNF beam will send 1.1×10^{21} protons on target (POT) each year in the direction of two detectors, near and far. The near detector (ND) is located 574 m away from the neutrinos' source and is composed of several subdetectors placed side by side, totaling 70 tons (fiducial mass) of liquid argon. The primary aims of the near detector is to characterize the flux produced while reducing systematic uncertainty in interaction rates at far detector. The far detector (FD) at the Sanford Underground Research Facility (SURF) in Lead, South Dakota, is 1297 km away from the neutrinos' source, which travels through the interior earth with a matter density of $\rho = 2.848$ g/cm^3. The far detector is a huge detector containing 40 kton of liquid argon (fiducial mass) that employs Liquid Argon Time Projection Chamber (LArTPC) technology. These configurations allow the DUNE experiment to investigate the τ-channel, which is not typically considered in neutrino oscillation analysis. Detecting tau is more difficult than detecting other charged leptons, hence all constraint parameters in the oscillation analysis are determined by the appearance and disappearance of $\nu_{\rm e}$ and ν_μ events. When we are studying oscillation neutrino is necessary identified and reconstructed both outgoing charged leptons and the energy of incoming neutrino in order to classify of events with respective flavor. Identified and reconstructed ν_τ interacts via a charged-current (CC) interaction is naturally more challenging than detected and reconstructed $\nu_{\rm e}$ and ν_μ events for a variety of reasons. Since that τ-lepton mass is larger than other charged leptons mass implies that threshold of the energy of incoming ν_τ to generate CC interaction with detector's medium is necessarily large. For occurs a CC interaction with nucleon ($\nu_\tau + N \rightarrow \tau + N'$) the energy of incoming ν_τ needed is $E_{\nu_\tau} \gtrsim 3.35$ GeV, so reducing of the statistic sample for a variety of experiments. Furthermore, reconstructing the τ-lepton in the neutrino detector is a greater challenge than that of other leptons. Even though liquid argon detectors have resolution of the around several millimeters and be great at reconstructing final-state particles. The τ-leptons decay promptly with a decay length significantly smaller than the resolution of liquid argon detectors. Therefore, the identification and reconstruction of τ-leptons occur by reconstruction of your decay products which always including a neutrino in the final-state ($\tau \rightarrow \nu_\tau + \text{something else}$). These facts become more difficult identifying a scattering event as a ν_τ CC interaction and so reject of neutral-current (NC) and also reconstructing the neutrino of incoming ν_τ. Around 65% of the τ-decays are hadronic [**?**], which an optimistically estimate predicted that 30% of hadronic τ-decay can be successfully identified while 0.5 % will be background [**?**], [**?**]. In spite of all challenges, the combination of a large ν_τ flux above the τ-production energy threshold and the capability of the argon liquid detector in reconstructing the final states makes the DUNE one the best experiment for detecting ν_τ samples. The DUNE simulation expects to collect a sample of 100 to 1000 events of ν_τ appearance within the experiment's window duration in the standard scenario, expected over 300 events for 3 + 3 + 1 [4]. Although this quantity may appear small, the amount of events expected by DUNE over the experiment's long-baseline current and the future, such as T2HK (Tokai to Hyper- Kamiokande). Therefore, the DUNE experiment offers an opportunity to study new physics involving the ν_τ-appearance oscillation channel. Similar to the paper [4], we will assume the three-massive-neutrinos paradigm and just considered the normal ordering (NO).

In the standard model (SM), the ν_τ production in the Fermilab is basically insignificant and can be ignored. The ν_τ samples will arise because of oscillation model $\nu_\mu \rightarrow \nu_\tau$ at the FD

$$\frac{d\mathscr{N}_{\mu\tau}}{dE_\nu^{\rm true}} = \sum_i^{\rm bins} \left(\phi_\mu^{\rm SM}\, \sigma_\tau^{\rm SM}\, P_{\mu\tau}^{\rm SM}\right)_i \ , \tag{7}$$

where $\phi_\mu^{\rm SM}$ is the flux of ν_μ from the source, $\sigma_\tau^{\rm SM}$ the cross section, and $P_{\mu\tau}^{\rm SM} \equiv P(\nu_\mu \rightarrow \nu_\tau)$ the oscillation probability. Note that the events in eq.(7) are divided into energy bins, where $i = \{1, 2, \cdots, \text{bins}\}$. The reconstructed events per energy bin

(E_ν^{reco}) from the true events per energy bin (E_ν^{true}) can be to map using a migration matrix

$$\frac{dN_{\mu\tau}}{dE_\nu^{\text{reco}}} = \int dE_\nu^{\text{true}} \, \frac{d\mathscr{N}_{\mu\tau}}{dE_\nu^{\text{true}}} \, f(E_{\text{reco}}, E_{\text{true}}) \, . \tag{8}$$

In general, the mapping $f(E_{\text{reco}}, E_{\text{true}})$ may be described using a Gaussian function that replicates the measurement of the detector taking into account your resolution as well as the bias and error in the reconstruction of the energy to incoming neutrinos. In other words, the quantity observed by detectors are the reconstructed events. We reproduced the reconstructed events from true events of the DUNE's simulates [4] using the Gaussian function

$$f(E_{\text{reco}}, E_{\text{true}}) = \exp\left[-\frac{1}{2}\left(\frac{E_\nu^{\text{reco}} - \mu_\nu^{\text{true}}}{\sigma_\nu^{\text{true}}}\right)^2\right] \, , \tag{9}$$

where $\mu_\nu^{\text{true}} = bE_\nu^{\text{true}}$ is the mean value and $\sigma_\nu^{\text{true}} = rE_\nu^{\text{true}}$ the width, being b and r the bias and the resolution of detector, respectively. The best fit we found is $b = XX$ and $r = YY$. As the last publication of global fit available by the NuFit collaboration is on September 2024 (v6.0)

$$\begin{gathered}\sin^2\theta_{12} = 0.307, \quad \sin^2\theta_{13} = 0.02195, \quad \sin^2\theta_{23} = 0.561, \quad \delta_{CP}/\pi = 0.98, \\ \Delta m^2_{21} = 7.49 \times 10^{-5}\ \text{eV}^2, \quad \Delta m^2_{31} = +2.534 \times 10^{-3}\ \text{eV}^2.\end{gathered} \tag{10}$$

We updated the simulated data in [4] considering the relation

$$\mathscr{N}_{(24)}^{\text{true}} = \phi_\mu^{\text{SM}} \, \sigma_\tau^{\text{SM}} \, P_{\mu\tau}^{(24)} = \frac{P_{\mu\tau}^{(24)}}{P_{\mu\tau}^{(18)}} \mathscr{N}_{(18)}^{\text{true}} \, , \tag{11}$$

where $\mathscr{N}_{(ij)}^{\text{true}}$ and $P_{\mu\tau}^{(ij)}$ represent the true events to FD eq.(7) and the oscillation probability $\nu_\mu \to \nu_\tau$, respectively, assuming the best-fits for the years 2018 or 2024 $\big(\text{adequately denotated}, (ij) = (18) \text{ or } (24)\big)$. To acquire the updated reconstructed events $\big(N_{(24)}^{\text{reco}}\big)$, we applied the Gaussian mapping eq.(9) in the updated true events eq.(11) through the eq.(8). We used the updated reconstructed events to carry out our analysis in section V. From now on, we omitted the upper and down indexes when there were no ambiguities.

The introduction of the CC NSI to the Lagrangian eq.(1) results in new channels for pion decay [Artigo], where we assume only the pseudo-scalar interaction $[\epsilon_P]_{\mu\tau} \equiv \epsilon_{\mu\tau}$ is not zero. This new channel violates the lepton flavor number, the μ-lepton can be associated with ν_τ as a sub-leading channel decay because $\epsilon_{\mu\tau} \neq 0$. As discussed in [Artigo] and can be observed in the eq.(2), even though the CC NSI modifies the flux of neutrinos flavor, we can summarize your effect modifying the oscillation probability. The flux and cross section remain the same as the SM. For the term $\epsilon_{\mu\tau}$ different of zero, the expression to NSI probability is very simplified

$$P_{\mu\tau}^{\text{NSI}} = \left|S_{\tau\mu}^{\text{SM}} - p_\mu \epsilon_{\mu\tau}^* S_{\tau\tau}^{\text{SM}}\right|^2 \, , \tag{12}$$

being $S_{\alpha\beta}^{\text{SM}}$ are the components $\alpha\beta = \{\tau\mu, \, \tau\tau\}$ of the evolution matrix in the SM, and $\epsilon_{\mu\tau}$ is the epsilon term from eq.(3) for $\alpha\beta = \{\mu\tau\}$, with the associated coefficient being represented by $p_\mu \equiv m_\pi^2 / \left(m_\mu(m_u + m_d)\right) \approx 27$. The flavor transition $\nu_\mu \to \nu_\tau$ is expresses via the NSI probability $P_{\mu\tau}^{\text{NSI}} \equiv \hat{P}(\nu_\mu \to \nu_\tau) = \hat{P}_{\mu\tau}$. We have used the hat on the NSI variables to differentiate them from the SM variables. Although we referred to the eq.(12) as probability, we emphasize that it can acquire values greater than unit. The NSI probability with material effect can be derived in a relatively simple perturbative analytical form [NOSSO] when utilized the perturbative expressions of the evolution matrix with material effect [MatrixSSM]. However, because we are interested in investigating how well the $\epsilon_{\mu\tau}$ can be constrained by DUNE's detectors, we considered a purely numerical approaching. In our analysis, the $\epsilon_{\mu\tau}$ is assumed to be real and is marginalized by the χ^2_{BC} function eq.(**??**) considering all the parameters oscillation fixed in the best-fit eq.(10), unless otherwise stated. Before we present the discussion of how we generated the NSI events to FD, we should computerize the NSI effect to ND, because the ND is used for restringing the uncertainties in the FD

$$N_{\mu\tau;\ \text{Far}}^{\text{Obs}} = \frac{N_{\mu\mu;\ \text{Near}}^{\text{Obs}}}{N_{\mu\mu;\ \text{Near}}^{\text{Mod}}} \, N_{\mu\tau;\ \text{Far}}^{\text{Mod}} = \frac{\hat{P}_{\mu\mu}^{\text{Near}}}{P_{\mu\mu}^{\text{Near}}} \, N_{\mu\tau;\ \text{Far}}^{\text{Mod}} \approx \hat{P}_{\mu\mu}^{\text{Near}} \, N_{\mu\tau;\ \text{Far}}^{\text{Mod}} \, , \tag{13}$$

where $N_{\alpha\beta;\ Y}^{X}$ are the reconstructed events by $Y = \{\text{Near, Far}\}$ detector to transition $\alpha \to \beta$ assuming the $X = \{\text{Mod, Obs}\}$ case, the prevision of model and the observable, respectively. The NSI effect should be present in the observable events. For motive of completeness, we considered the relation eq.(13) in our analysis; however, the effect is irrelevant for this case. As we desire obtain the observable events in the FD with the NSI effect included, we should consider the expected reconstructed

NSI events from application of the migration matrix under the true NSI events. The true NSI events are obtained by theoretical NSI model

$$\frac{d\hat{\mathcal{N}}_{\mu\tau}}{dE_\nu^{\text{true}}} = \sum_i^{\text{bins}} \left(\phi^{\text{SM}}\sigma^{\text{SM}}\hat{P}_{\mu\tau}\right)_i = \frac{\hat{P}_{\mu\tau}}{P_{\mu\tau}}\frac{d\mathcal{N}_{\mu\tau}}{dE_\nu^{\text{true}}}\,, \tag{14}$$

where $\mathcal{N}_{\mu\tau}$ are the true events given in eq.(11) to FD. Therefore, the reconstructed NSI events to FD are obtained applying the migration matrix eq.(9) in the eq.(14), analogous the eq.(8), and substituting in the eq.(13)

$$\frac{d\hat{N}_{\mu\tau}}{dE_\nu^{\text{reco}}} = \hat{P}_{\mu\mu}^{\text{Near}} \int dE_\nu^{\text{true}}\, \frac{d\hat{\mathcal{N}}_{\mu\tau}}{dE_\nu^{\text{true}}}\, f(E_{\text{reco}}, E_{\text{true}})\,. \tag{15}$$

In a similar way to [4], we divided the reconstructed events into 40 energy bins ranging from 0 and 20 GeV, with a constant width of $\Delta E_\nu = 0.5$ GeV. The reconstructed SM events to FD eq.(8) are illustrated in the Upper Figure 5 for all the oscillation parameters fixed by eq.(10). The left (middle) graphic shows the $\nu_\tau(\bar{\nu}_\tau)$-sample to the contributions of $\tau^\pm$-reconstruction and the NC background events for neutrino (antineutrino) mode. The right graphic illustrates the reconstructed SM events for high-energy mode. Similarly, we plot three values different for $\epsilon_{\mu\tau}$ exclusively neutrino mode in order to illustrate how the NSI effect modifies the reconstructed events in the Lower Figure 5. From left to right, we explored $\epsilon_{\mu\tau} = X1, X2, X3$ while maintaining the others oscillation parameters fixed by eq.(10).

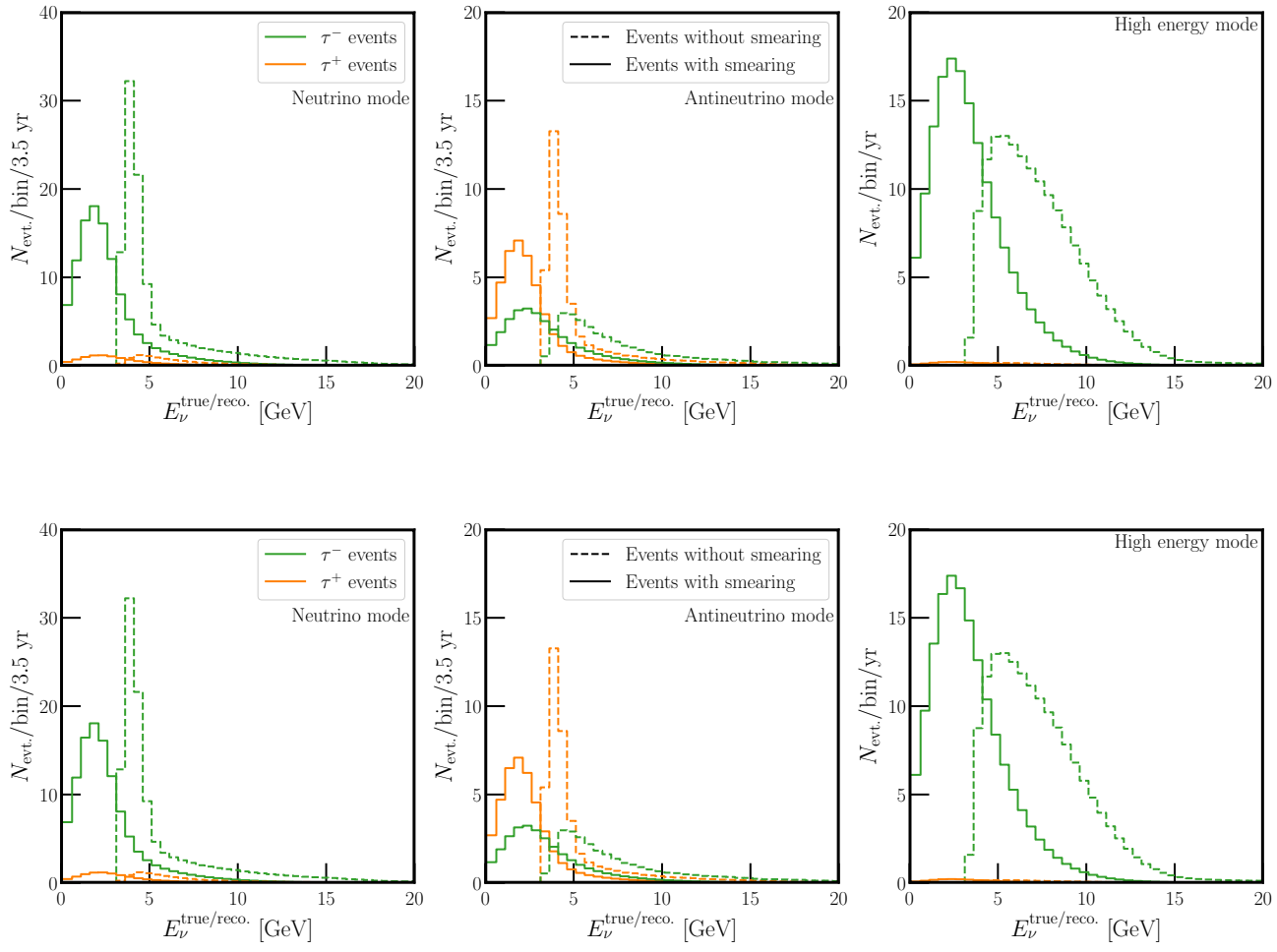

FIG. 5. Upper: Events_SM Lower: Events_NSI

We also realized a study about $\epsilon_{\mu\tau}$'s constraint delimited by the ND's sensibility. Assuming that the flux can be described using spherical symmetry and that the efficiency in ND and FD differ only because the fiducial masses differ. We can calculate

the events at ND employing a geometry factor

$$\kappa = \frac{\phi^{\rm SM}_{\mu;\,\rm Near}}{\phi^{\rm SM}_{\mu;\,\rm Far}} \frac{\sigma^{\rm SM}_{\tau;\,\rm Near}}{\sigma^{\rm SM}_{\tau;\,\rm Far}} = \frac{M_{\rm Near}}{M_{\rm Far}} \frac{L^2_{\rm Far}}{L^2_{\rm Near}} \,, \tag{16}$$

where for the DUNE's $Y = \{\,\text{Near, Far}\}$ detector the variable $\phi^{\rm SM}_{\mu;\,Y}$ denotes the ν_μ flux at respective detector, $\sigma^{\rm SM}_{\tau;\,Y}$ the cross section for ν_τ, M_Y the fiducial mass, and L^2_Y the distance source-detector. Using data from DUNE's collaboration [DUNE'Colla], we calculated the ratio of near and far fluxes in order to cross-check the $\kappa/\Delta\sigma^{\rm SM}_\tau$ value, where we denote $\Delta\sigma^{\rm SM}_\tau = \sigma^{\rm SM}_{\tau;\,\rm Near}/\sigma^{\rm SM}_{\tau;\,\rm Far}$. The $\kappa/\Delta\sigma^{\rm SM}_\tau$ constant coincided relatively well with the average ratio of near and far fluxes. As a result, the true SM and NSI events at the ND can be estimated from the respective true events at the FD using the relations

$$\frac{d\mathscr{N}^{\rm Near}_{\mu\tau}}{dE^{\rm true}_\nu} = \sum_i^{\rm bins} \left(\phi^{\rm SM}_{\mu;\,\rm Near}\, \sigma^{\rm SM}_{\tau;\,\rm Near}\, P^{\rm Near}_{\mu\tau}\right)_i = \kappa\, \frac{P^{\rm Near}_{\mu\tau}}{P_{\mu\tau}}\, \frac{d\mathscr{N}_{\mu\tau}}{dE^{\rm true}_\nu} \,, \tag{17}$$

$$\frac{d\hat{\mathscr{N}}^{\rm Near}_{\mu\tau}}{dE^{\rm true}_\nu} = \sum_i^{\rm bins} \left(\phi^{\rm SM}_{\mu;\,\rm Near}\, \sigma^{\rm SM}_{\tau;\,\rm Near}\, \hat{P}^{\rm Near}_{\mu\tau}\right)_i = \kappa\, \frac{\hat{P}^{\rm Near}_{\mu\tau}}{P_{\mu\tau}}\, \frac{d\mathscr{N}_{\mu\tau}}{dE^{\rm true}_\nu} \,, \tag{18}$$

where $\mathscr{N}_{\mu\tau}$ are the true SM events at the FD eq.(11). The upper (lower) relation eq. (17) (eq.(18)) generates true SM (NSI) events at the ND. Because the FD and ND detectors are the same nature, we assuming that the reconstructed events at the ND are produced by the same Gaussian function as the FD. To produce the reconstructed SM and NSI events at the ND, we used the migration matrix eq.(9) in the eq.(17) and eq.(18), respectively

$$\frac{dN^{\rm Near}_{\mu\tau}}{dE^{\rm reco}_\nu} = \int dE^{\rm true}_\nu\, \frac{d\mathscr{N}^{\rm Near}_{\mu\tau}}{dE^{\rm true}_\nu}\, f(E_{\rm reco}, E_{\rm true}) \,, \tag{19}$$

$$\frac{d\hat{N}^{\rm Near}_{\mu\tau}}{dE^{\rm reco}_\nu} = \int dE^{\rm true}_\nu\, \frac{d\hat{\mathscr{N}}^{\rm Near}_{\mu\tau}}{dE^{\rm true}_\nu}\, f(E_{\rm reco}, E_{\rm true}) \,. \tag{20}$$

We used the reconstructed events to develop our static analysis of $\epsilon_{\mu\tau}$'s constraint for both near and far detectors. The analyses are performed using the $\chi^2_{\rm BC}$ function eq. (**??**), where the details can be found in the section V.

IV. FURTHER CONSTRAINTS

We used these DUNE experiment features to see how effectively we could constrain the NSI parameter in pion decay for both near and far detectors using the description offered in the previous section.

explain other constraints such as far detector at DUNE, fluxes with muoninc neutrino. Also T2K and NOVA. Also pion decay

efeito aqui é devido diminuição neutrinos eletronicos ou muonicos

In the last section we have seen how the inclusion of the CC NSI $\epsilon_{\mu\tau}$ will modify the event rates of tau neutrinos, to be measured at DUNE. However, a non-null CC NSI will also impact other channels, such as the electron appearance ($\nu_\mu \to \nu_e$) and muon disappearance ($\nu_\mu \to \nu_\mu$). This can be easily understood by observing Eq. (2)

V. NUMERICAL RESULTS

present the results, mainly the chi2 plot.
checar elipse e minimo local

ABCD

** **Ed** **: We used these DUNE experiment features to see how effectively we could constrain the NSI parameter in pion decay for both near and far detectors using the description offered in the previous section.

VI. CONCLUDING REMARKS

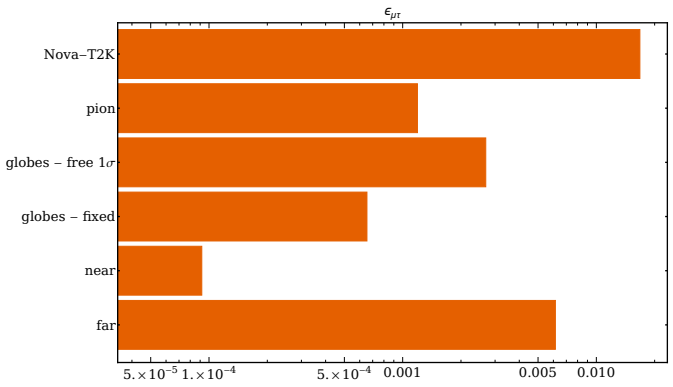

FIG. 6. $\chi^2 < 3.84$

Appendix A: Motivation

In the paper from Andre de Gouvea *et al.* (1904.07265)[4], they compute the number of tau neutrinos in the far detector (fig.2 in the paper). Here the Figure(8). The figure has two curves, one for the true energy of the incident neutrino (dashed) and the other for the reconstructed energy(solid). The decay chain is something like:

$$\nu_\tau N \to \tau + X \tag{A1}$$

where $\tau \to \nu_\tau +$ hadron or $\tau \to \nu_\tau + \ell_\alpha + \nu_\alpha$ for α may represent either the electron or muon flavor, as can be seen in fig. 7. We do not measure the tau, only the hadronic debris. Therefore, we cannot reconstruct the energy of the incident neutrino

Decay mode	Meson resonance	$\mathcal{B}$ [%]	
$\tau^- \to e^- \overline{\nu}_e \nu_\tau$		17.8	
$\tau^- \to \mu^- \overline{\nu}_\mu \nu_\tau$		17.4	
$\tau^- \to h^- \nu_\tau$		11.5	1 prong ~47%
$\tau^- \to h^- \pi^0 \nu_\tau$	$\rho(770)$	26.0	
$\tau^- \to h^- \pi^0 \pi^0 \nu_\tau$	$a_1(1260)$	9.5	
$\tau^- \to h^- h^+ h^- \nu_\tau$	$a_1(1260)$	9.8	3 prongs ~15%
$\tau^- \to h^- h^+ h^- \pi^0 \nu_\tau$		4.8	
Other modes with hadrons		3.2	
All modes containing hadrons		64.8	

FIG. 7. Different type rate probabiity of the tau decay.

very well (part of the energy is lost in the final neutrino). This explains why the solid curves are to the left of the dashed ones. For the plots, we have

$$N^{\rm SM}_{\rm events} = \phi_\mu P(\nu_\mu \to \nu_\tau)\sigma_\tau \tag{A2}$$

since in the SM, there is no tau neutrino at source. So, the tau neutrino only appears at the far detector through conversion. In our model, we have

$$P^{\rm NSI}_{\mu\beta} = \left| S^{\rm SM}_{\beta\mu} - p_\mu \epsilon^*_{\mu i} S^{\rm SM}_{\beta i} \right|^2, \tag{A3}$$

where we have a sum over i.

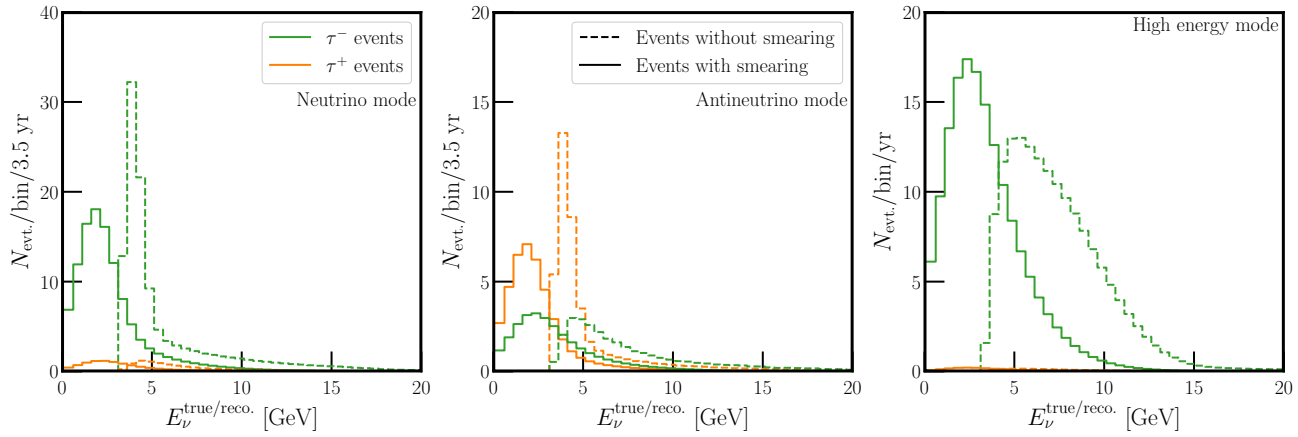

FIG. 8. Expected number of ν_τ-identified signal events per 0.5 GeV bin as a function of the true (dashed) or reconstructed (solid) neutrino energy. The left panel displays the expected number of events when in neutrino mode, the center panel displays the antineutrino mode, and the right panel displays high-energy mode events. In each panel, we show the contribution due to neutrinos in green and antineutrinos in orange. Each distribution has been normalized to the expected run-time in each mode, 3.5 years for neutrino and antineutrino modes and 1 year for high-energy mode.

Appendix B: The model

The EFT Lagrangian that modifies the neutrino interactions is defined by [1]

$$\begin{aligned}\mathscr{L}_{\rm WEFT} \supset -\frac{2\,V_{jk}^{CKM}}{v^2}\Big\{&[1+\epsilon_L^{jk}]_{\alpha\beta}\left(\bar{u}^j\gamma^\mu P_L d^k\right)\left(\bar{\ell}_\alpha\gamma_\mu P_L\nu_\beta\right)+[\epsilon_R^{jk}]_{\alpha\beta}\left(\bar{u}^j\gamma^\mu P_R d^k\right)\left(\bar{\ell}_\alpha\gamma_\mu P_L\nu_\beta\right)\\&+\frac{1}{2}\left[\epsilon_S^{jk}\right]_{\alpha\beta}\left(\bar{u}^j d^k\right)\left(\bar{\ell}_\alpha P_L\nu_\beta\right)-\frac{1}{2}\left[\epsilon_P^{jk}\right]_{\alpha\beta}\left(\bar{u}^j\gamma^5 d^k\right)\left(\bar{\ell}_\alpha P_L\nu_\beta\right)\\&+\frac{1}{4}\left[\epsilon_T^{jk}\right]_{\alpha\beta}\left(\bar{u}^j\sigma^{\mu\nu} P_L d^k\right)\left(\bar{\ell}_\alpha\sigma_{\mu\nu} P_L\nu_\beta\right)+\text{h.c.}\Big\}\,.\end{aligned}\tag{B1}$$

Here, V^{CKM} is the Cabibbo-Kobayashi-Maskawa (CKM) matrix, $v = 1/(\sqrt{2}G_F) \approx 246\,\text{GeV}$ is the vacuum expectation value of the SM Higgs field and ϵ_X are the Wilson coeficients, with $X = L, R, S, P, T$ for left-handed, right-handed, scalar, pseudo-scalar and tensor, respectively. The Roman (Greek) symbols denote the quark (lepton) generations. This Lagrangian is based on the Weak Effective Field Theory (WEFT), that acts bellow electroweak scale [2].

For simplicity, we only study $(\epsilon_P)_{\alpha\beta}$ which we will denote as $\epsilon_{\alpha\beta}$.

Appendix C: Methodology

We have extracted from the plots of fig. A the number of true events as well as the reconstructed ones for all channels. The latter is only needed for cross-check. Using the number of true events as input, we have obtained the reconstructed events by ourselves. This was achieving by a smearing function given by

$$f(E_{\rm rec}, E_{\rm true}) = \exp\left[-\frac{1}{2}\left(\frac{E_{\rm rec} - bE_{\rm true)}}{rE_{\rm true}}\right)^2\right]\tag{C1}$$

where $b = 0.45$, and $r = 0.25$.

Explicitly,

$$\frac{dN_{\rm events}}{dE_\nu^{\rm reco}} = \int \mathrm{d}E_\nu^{\rm true}\frac{dN_{\rm events}}{dE_\nu^{\rm true}} f(E_{\rm rec}, E_{\rm true})\tag{C2}$$

We have checked that the points reconstructed by ourselves in this way agree with the reconstructed points of the plots of fig A. Normalization factors were added, to guarantee that the total number of reconstructed events is the same as the true events.

In the plots, the following parameters were fixed

$$\sin^2\theta_{12} = 0.307; \quad \sin^2\theta_{13} = 0.02195; \quad \sin^2\theta_{23} = 0.561;$$
$$\delta_{\rm CP} = 3.08923\ {\rm rad} \quad \Delta m^2_{21} = 7.49\times10^{-5}{\rm eV}^2 \quad \Delta m^2_{31} = 2.534\times10^{-3}{\rm eV}^2 \tag{C3}$$

The baseline is 1300km for DUNE as well as the matter density is $\rho = 2.848 g/cm^3$.

It is possible to obtain the number of events for other values by re-scaling as below

$$\frac{dN_{\rm events}(\hat{x})}{dE_\nu^{\rm true}} = \phi_\mu P^{\hat{x}}_{\mu\tau}\sigma_\tau = \frac{P^{\hat{x}}_{\mu\tau}}{P^{x}_{\mu\tau}}\frac{dN_{\rm events}(x)}{dE_\nu^{\rm true}} \tag{C4}$$

where x is a vector with the parameters defined in Eq. (C3), while $\hat{x}$ is a vector with a different choice for any of the parameters. In the presence of NSI, it is still possible to obtain a perturbative formula for the conversion probability. Or one can resort to numerical methods. In any case, it is straightforward to obtain the event rates for any chosen value of the standard parameters or/and NSI.

Once the number of events from CC is known, we have to add the background (NC). It can be extracted from the figure (black region)

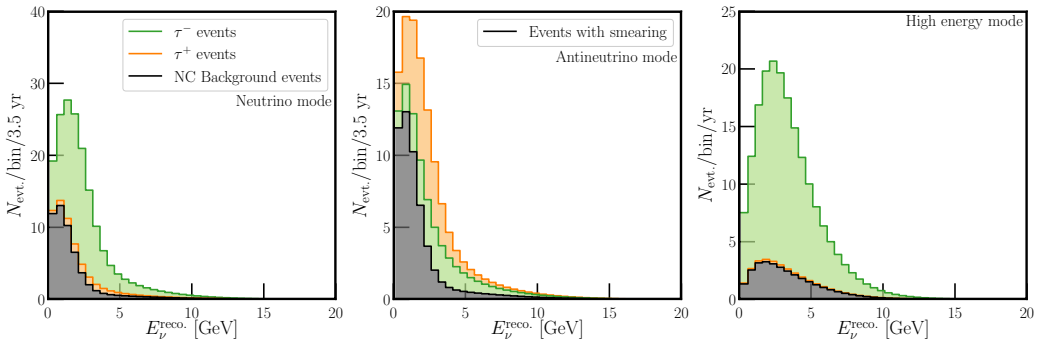

FIG. 9. Caption

Finally, the chi square function is given by

$$\chi^2 = \sum_i n_{i,teo} - n_{i,data} + n_{i,data}\log\left(\frac{n_{i,data}}{n_{i,teo}}\right) + \left(\frac{\alpha}{\sigma}\right)^2 \tag{C5}$$

where $n_{i,teo} = N_i^{NSI} = N_{i,CC}^{NSI} + (1+\alpha)N_{i,NC}^{NSI}$, and $n_{i,data} = N_i^{SM} = N_{i,CC}^{SM} + N_{i,NC}^{SM}$. We also chose $\sigma = 0.25$

The above analysis was applied to study the sensitivity on $\epsilon_{\mu\tau}$. Fixing the values of the standard parameters as in Eq. (C3) we obtained the result of fig. 10.(preliminary result)

The current bound (from pion decay) is around 2×10^{-3} at 90%C.L. [2]. The sensitivity from DUNE is at least one order of magnitude higher.

We can also study the sensitivity at the near detector. In this case, we can obtain the number of events by the formula

$$\frac{dN^{near}_{\rm events}(\hat{x})}{dE_\nu^{\rm true}} = \phi^{near}_\mu P^{\hat{x}}_{\mu\tau}\sigma_\tau = \frac{P^{\hat{x}}_{\mu\tau}}{P^{x}_{\mu\tau}}\frac{\phi^{near}_\mu}{\phi^{far}_\mu}\frac{dN_{\rm events}(x)}{dE_\nu^{\rm true}} \tag{C6}$$

We will approximate the flux as spherically symmetry, so $N = \int \phi^{total} dA \to \phi^{total} = N/(4\pi r^2)$. Moreover, the detector can only see a fraction of the flux. Thus,

$$\frac{\phi^{near}_\mu}{\phi^{far}_\mu} = \frac{N_{near}/(4\pi r^2_{near})}{N_{far}/(4\pi r^2_{far})} = \frac{N_{near}}{N_{far}}\frac{r^2_{far}}{r^2_{near}} \equiv \kappa \tag{C7}$$

We will consider that $L_{near} = 1$km, and that the near detector will contain 70 ton while $N_{\rm far}$ = 40 kton. This is particularly interesting, since the standard event rate is very small. We obtain the result of fig. 11preliminary result

From the result above, DUNE could increase the sensitivity on $\epsilon_{\mu\tau}$ one order of magnitude. preliminary

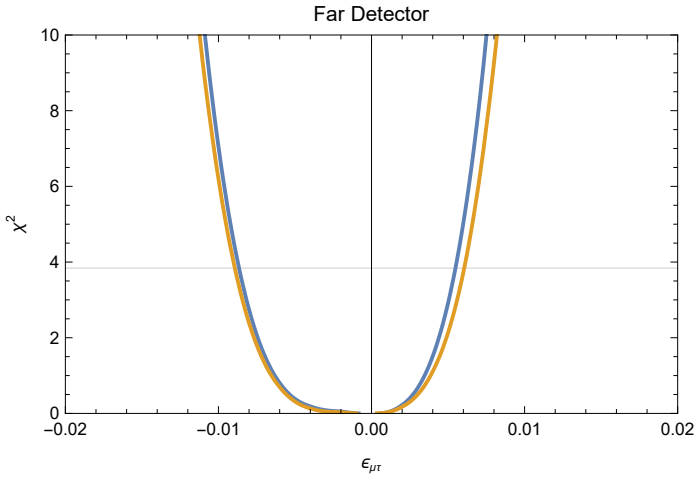

FIG. 10. Sensitivity on $\epsilon_{\mu\tau}$ at the far detector, considering running of 3. years at neutrino mode, 3. years at anti-neutrino mode, and 1 year at high-energy mode. The line is for 95%C.L. The blue line is without background and the orange line is including background.

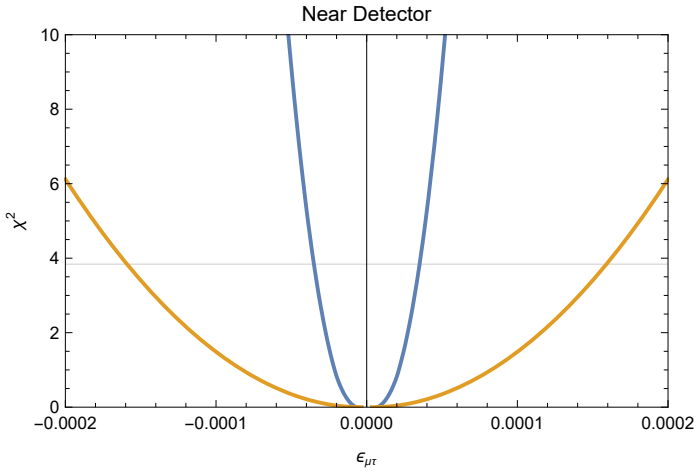

FIG. 11. Sensitivity on $\epsilon_{\mu\tau}$ at the near detector, considering running of 3. years at neutrino mode, 3. years at anti-neutrino mode, and 1 year at high-energy mode. The line is for 95%C.L. The blue line is without background and the orange line is including background.

When computing the result for the far detector, we are implicitly using the normalization for fluxes (of muon neutrino) in the SM. Since the fluxes change, we have to take this into account as well.

Recall that we defined

$$\frac{dN^{\rm near}_{\rm events}(\hat{x})}{dE^{\rm true}_{\nu}} = \phi^{near}_{\mu}(x) P^{\hat{x}}_{\mu\tau}\sigma_{\tau} \tag{C8}$$

however, we should have used

$$\frac{dN^{near}_{\rm events}(\hat{x})}{dE^{\rm true}_{\nu}} = \phi^{near}_{\mu}(\hat{x}) P^{\hat{x}}_{\mu\tau}\sigma_{\tau} = \frac{P^{\hat{x}}_{\mu\mu}}{P^{x}_{\mu\mu}}\phi^{near}_{\mu}(x) P^{\hat{x}}_{\mu\tau}\sigma_{\tau} \tag{C9}$$

$$\frac{dN^{far}_{\rm events}(\hat{x})}{dE^{\rm true}_{\nu}} = \phi^{far}_{\mu}(\hat{x}) P^{\hat{x}}_{\mu\tau}\sigma_{\tau} = \frac{\phi^{far}_{\mu}(\hat{x})}{\phi^{near}_{\mu}(\hat{x})}\frac{\phi^{near}_{\mu}(\hat{x})}{\phi^{near}_{\mu}(x)}\frac{\phi^{near}_{\mu}(x)}{\phi^{far}_{\mu}(x)}\phi^{far}_{\mu}(x) P^{\hat{x}}_{\mu\tau}\sigma_{\tau} \tag{C10}$$

$$= \kappa^{-1}\,\frac{P^{\hat{x}}_{\mu\mu}}{P^{x}_{\mu\mu}}\,\kappa\,\phi^{far}_{\mu}(x) P^{\hat{x}}_{\mu\tau}\sigma_{\tau} = \frac{P^{\hat{x}}_{\mu\mu}}{P^{x}_{\mu\mu}}\,\phi^{far}_{\mu}(x) P^{\hat{x}}_{\mu\tau}\sigma_{\tau} \tag{C11}$$

We have also checked what is the ratio ϕ^{near}/ϕ^{far} using the implementation in GLOBES of DUNE [**?**], see fig 12. In the figure, the red line is for $(1300/1)^2$, while the green line is for $(1297/0.574)^2$ which are the values used in GLOBES

implementation (see section II of [**?**]). The energy displayed in the plots is the true energy. Moreover, our choice to use only geometric factors is conservative for most of the points (the points are above the green line).

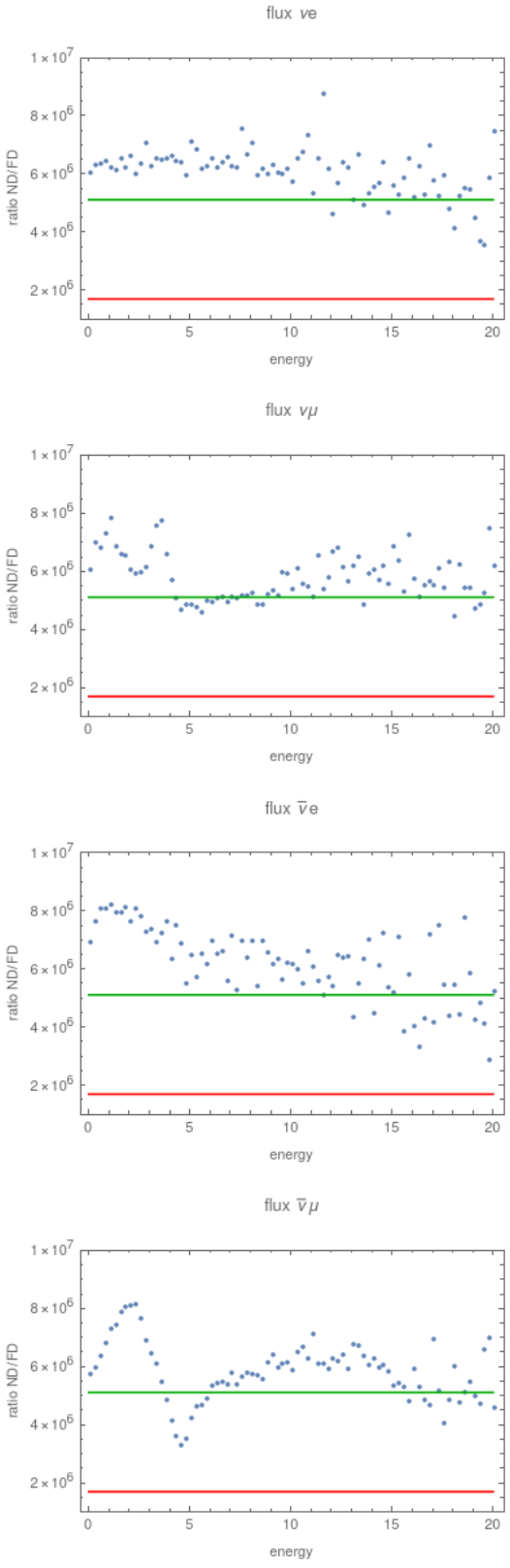

FIG. 12. Ratio flux near/far from DUNE

Using GLOBES, we can also study which is the sensitivity on $\epsilon_{\mu\tau}$. The results are given in figures 13-14. In fig. 13, the standard parameters are fixed in the best-fit check values, while in fig. 14 the std parameters are allowed to vary at 1sg, need checking. In GLOBES, they consider 10 years, not 7 as we are doing. There is not high energy as well.

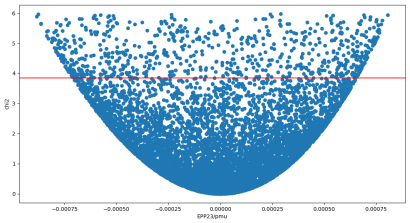

FIG. 13. Fixed std

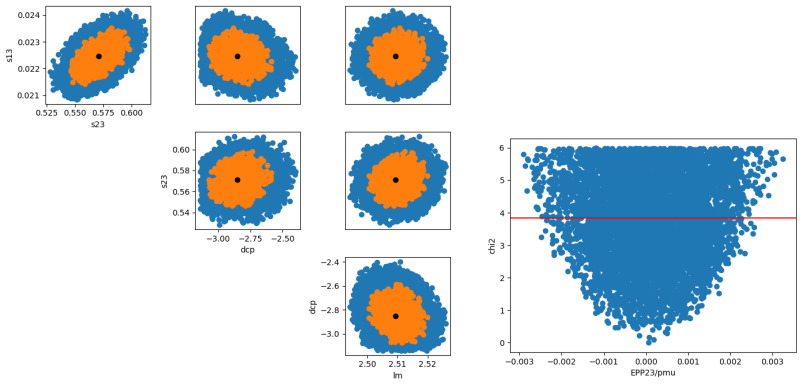

FIG. 14. Free std

Next job is to study the disapparence rate, how it change with NSI.

Appendix D: Neutrino transition rate

Copied from 2309.15924

In this work we will adopt the more general QFT framework to describe neutrino oscillations in long-baseline experiments, following [1] (see also [5–7] for previous treatment in QFT not including NSI). The main point is to consider the entire process (from neutrino production to its detection) as an unique process in QFT. Thus, the differential event rate for neutrinos of flavor β with energy E_ν to be detected at a distance L from the source S, where they were produced with flavor α, is given by

$$R^S_{\alpha\beta} = \frac{N_T}{32\pi L^2 m_S m_T E_\nu} \sum_{k,l} e^{-i\frac{L\Delta m^2_{kl}}{2E_\nu}} \int d\Pi_{P'} \mathscr{M}^P_{\alpha k} \overline{\mathscr{M}}^P_{\alpha l} \int d\Pi_D \mathscr{M}^D_{\beta k} \overline{\mathscr{M}}^D_{\beta l} \,, \tag{D1}$$

where N_T is the number of target particles, $m_{S,T}$ are the masses of the source and target particles respectively, and we denote complex conjugation with a bar. As usual, $\Delta m^2_{kl} \equiv m^2_k - m^2_l$ denotes the difference of neutrino masses squared, while the phase-space integrals are given by $d\Pi \equiv \frac{d^3k_1}{(2\pi)^3 2E_1} \cdots \frac{d^3k_n}{(2\pi)^3 2E_n} (2\pi)^4 \delta^4(\sum p_n - \sum k_i)$. Here, we denote by k_i and E_i the four-momenta and energies of the final states, while the sum $\sum p_n$ amounts to the total four-momentum of the initial state. Since we are interested in the differential number of events per incident neutrino energy E_ν, we actually define $d\Pi_P \equiv d\Pi_{P'} dE_\nu$, as can be seen in eq.(D1). Notice also that we are considering oscillation in vacuum only. Matter effects will be taken into account below.

As already stated, we will focus on long-baseline experiments, in which neutrinos are mainly produced by pion decay. Moreover, we will only consider beyond the SM (BSM) possible effects at neutrino production and/or propagation (by interaction with the medium). This is justified by the complicated nature of detection in long-baseline experiments. To properly include BSM effects, it would require first a theoretical description of standard neutrino interaction with nucleus, which is still not

satisfactory [8](see appendix **??** a brief description of the present status). Thus, regarding the detection amplitude, $\mathscr{M}^D_{\beta k}$, it will be given by

$$\mathscr{M}^D_{\beta k} = U_{\beta k} A^D \,, \tag{D2}$$

where A^D is a reduced matrix element whose explicit form is not relevant, and U_{ij} is the PMNS matrix.

As recently pointed out [3], in the presence of BSM effects care must be exercised when calculating the phase-space integral related to the production amplitude. The amplitude concerning pion decay, $\pi^+ \to \ell^+_\alpha \nu_k$, is given by [3]

$$\mathscr{M}^{P,\pi}_{\alpha k} \equiv \mathscr{M}(\pi^+ \to \ell^+_\alpha \nu_k) = -i\, m_\mu f_{\pi^\pm} \frac{V_{ud}}{v^2} [\mathscr{P} U]^*_{\alpha k} (\bar{u}_{\nu_k} P_L v_{\ell_\alpha}) \,, \tag{D3}$$

where $f_{\pi^\pm}$ is the pion decay constant, v_{ℓ_α}, $\bar{u}_{\nu_k}$ are the Dirac spinor wave functions of the charged lepton and the neutrino, respectively, and we are using the notation

$$[\mathscr{P}]_{\alpha\beta} \;\equiv\; \delta_{\alpha\sigma} + \bar{\epsilon}_{\alpha\sigma}, \quad \text{where} \quad \bar{\epsilon}_{\alpha\sigma} = (\epsilon_L)_{\alpha\sigma} - (\epsilon_R)_{\alpha\sigma} - \frac{m^2_{\pi^\pm}}{m_{\ell_\alpha}(m_u + m_d)} (\epsilon_P)_{\alpha\sigma} \,. \tag{D4}$$

The NSI $\epsilon_L, \epsilon_R, \epsilon_P$ are defined in eq.(**??**). As can be seen, $\bar{\epsilon}_{\alpha\sigma}$ actually encodes the deviation from the PMNS matrix U due to the presence of NSI.

At first sight, one could insert eq.(D3) into eq.(D1), perform the phase-space integration, and obtain that BSM effects appear only in the numerator of eq.(D1). However, this reasoning is incorrect, since we are assuming the BSM presence in all cases that the pion decay is involved, related (or not) to experiments that aim to probe neutrinos properties. Therefore, we should re-express eq.(D3) in terms of the experimental measured decay width of the pion, which was already affected by BSM effects as well. Proceeding this way, we obtain [3]

$$\int d\Pi_{P'} \mathscr{M}^{P,\pi}_{\alpha k} \bar{\mathscr{M}}^{P,\pi}_{\alpha l} = 2\, m_{\pi^\pm} \Gamma_{\pi \to \ell_\alpha \nu} \frac{[\mathscr{P} U]_{\alpha l} [U^\dagger \mathscr{P}^\dagger]_{k\alpha}}{[\mathscr{P}\mathscr{P}^\dagger]_{\alpha\alpha}} \, \delta\Big(E_\nu - E_{\nu,\pi}\Big) \,, \tag{D5}$$

where $E_{\nu,\pi} = (m^2_{\pi^\pm} - m^2_\alpha)/(2m_{\pi^\pm})$ stands for the energy of the neutrino emitted. Finally, we can write eq.(D1) in the form

$$R^S_{\alpha\beta} = N_T \sigma^{\rm SM}_\beta(E_\nu) \Phi^{\rm SM}_\alpha(E_\nu) \sum_{k,l} e^{-i\frac{L\Delta m^2_{kl}}{2E_\nu}} \frac{[\mathscr{P} U]_{\alpha l} [U^\dagger \mathscr{P}^\dagger]_{k\alpha}}{[\mathscr{P}\mathscr{P}^\dagger]_{\alpha\alpha}} U_{\beta k} U^*_{\beta l} \,, \tag{D6}$$

where $\Phi^{\rm SM}_\alpha$ is the SM flux (with the decay width of the pion, $\Gamma_{\pi\to\ell_\alpha\nu}$, as input), while $\sigma^{\rm SM}_\beta$ is the SM cross-section. Notice that, by including the indirect effects (the denominator in $R^S_{\alpha\beta}$), there is no sensitivity to diagonal-only NSI.

Appendix E: TO DO

- We can re-scale the plots simply by doing

$$N^{\rm NSI}_{\rm events} = \phi_\mu P^{\rm NSI}_{\mu\tau} \sigma_\tau = \frac{P^{\rm NSI}_{\mu\tau}}{P^{\rm SM}_{\mu\tau}} N^{\rm SM}_{\rm events} \tag{E1}$$

  So the first step is to compute the ratio $\frac{P^{\rm NSI}_{\mu\tau}}{P^{\rm SM}_{\mu\tau}}$ using the oscillation parameters in the paper as a function of the energy. They used

$$\begin{gathered} \sin^2\theta_{12} = 0.310; \quad \sin^2\theta_{13} = 0.02240; \quad \sin^2\theta_{23} = 0.582; \\ \delta_{\rm CP} = -2.50{\rm rad} \quad \Delta m^2_{21} = 7.39\times10^{-5}{\rm eV}^2 \quad \Delta m^2_{31} = 2.525\times10^{-3}{\rm eV}^2 \end{gathered} \tag{E2}$$

  The baseline is 1300km for DUNE. We only need the value for the matter in the case of DUNE. I am using $\rho = 2.848 g/cm^3$.

- From reference [] we have **We divide the simulated data in energy bins of constant width $\Delta E_\nu = 0.5$ GeV, between 0 and 20 GeV, for our analyses**.

- Need to relate the plot with the reconstructed and true energy. Gaussian transformation?
  The differential rate

$$\frac{dN_{\rm events}^{\rm NSI}}{dE_\nu^{\rm true}} = \phi_\mu P_{\mu\tau}^{\rm NSI}\sigma_\tau = \frac{P_{\mu\tau}^{\rm NSI}}{P_{\mu\tau}^{\rm SM}}\frac{dN_{\rm events}^{\rm SM}}{dE_\nu^{\rm true}} \tag{E3}$$

in terms of true energy and the differential rate

$$\frac{dN_{\rm events}^{\rm NSI}}{dE_\nu^{\rm true}} = \phi_\mu P_{\mu\tau}^{\rm NSI}\sigma_\tau = \frac{P_{\mu\tau}^{\rm NSI}}{P_{\mu\tau}^{\rm SM}}\frac{dN_{\rm events}^{\rm SM}}{dE_\nu^{\rm true}} \tag{E4}$$

are connected by

$$\frac{dN_{\rm events}^{\rm NSI}}{dE_\nu^{\rm reco}} = \int \frac{dN_{\rm events}^{\rm NSI}}{dE_\nu^{\rm true}}\frac{{\rm d}\mathscr{R}}{{\rm d}E_\nu^{\rm reco}}(E_\nu^{\rm reco}, E_\nu^{\rm true})\,{\rm d}E_\nu^{\rm true} \tag{E5}$$

where

$$\frac{{\rm d}\mathscr{R}}{{\rm d}E_\nu^{\rm reco}}(E_\nu^{\rm reco}, E_\nu^{\rm true}) = \frac{1}{\sqrt{2\pi}\,\sigma_E}\exp\left[-\frac{1}{2}\left(\frac{E_\nu^{\rm reco}-bE_\nu^{\rm true}}{\sigma_E}\right)^2\right] \tag{E6}$$

with $\sigma_E = rE_\nu^{\rm true}, b = 0.45, r = 0.25$
For an explanation of reconstructed and true energy[3]

1. List to do

1) update FAR: L = 1297 Km and coefficient $\phi_{\mu\mu}$
   - first: update only L (fixed par. in the BF)
   - follow: include coefficient $\phi_{\mu\mu}$ (fixed par. in the BF)
   - BF nufit v5.3: nufit
   - see late: 3+3+1 and 3.5+3.5
2) update NEAR: L = 574 m
3) To do table of the limit sensitivity for pion decay (Leo's program)

OBS: Assuming BF simulated for NOvA+T2K

OBS: Parameters of the NutFit 6.0 (2024) (without SK atmospheric data)

$$\sin^2\theta_{12} = 0.307, \quad \sin^2\theta_{23} = 0.561, \quad \sin^2\theta_{13} = 0.02195,$$
$$\delta_{CP} = 177^\circ = 3.08923\ {\rm rad}\ ({\rm or}\ \delta_{CP}/\pi = 0.983333), \quad \frac{\Delta m_{21}^2}{10^{-5}\ {\rm eV}^2} = 7.49, \quad \frac{\Delta m_{31}^2}{10^{-3}\ {\rm eV}^2} = 2.534\,. \tag{E7}$$

[3] From GLOBES manual [9], section 10.1 we have the explanation of reconstructed and true energy.

Appendix A: EXTRA

in [4] they have (appendix A)

$$\sigma_E = 7\% \left(\frac{E_\nu}{1\mathrm{GeV}} \right) + 3.5\% \sqrt{\frac{E_\nu}{1\mathrm{GeV}}} \tag{A1}$$

For example in [10] they quote the following function

$$\frac{\mathrm{dR}}{\mathrm{d}N_h} = \frac{1}{\sqrt{2\pi}\,\sigma_h(T_e)} \exp\left[-\frac{1}{2} \left(\frac{N_h - \bar{N}_h(T_e)}{\sigma_h(T_e)} \right)^2 \right] \tag{A2}$$

As an example they use

$$\sigma_h(\bar{N}_h) = 1.21974 + 1.60121\sqrt{\bar{N}_h} - 0.14859\bar{N}_h. \tag{A3}$$

the transformation between reconstructed energy and true energy is given by

$$S^f_{N_h} = \int \frac{\mathrm{d}S^f_s}{\mathrm{d}T_e}(T_e)\, \frac{\mathrm{d}\mathscr{R}}{\mathrm{d}N_h}(T_e, N_h)\, \mathrm{d}T_e \tag{A4}$$

For us $\frac{\mathrm{d}S^f_s}{\mathrm{d}T_e}(T_e)$ is the spectrum as function of true energy, $S^f_{N_h}$ is spectrum in terms of reconstructed energy and $\frac{\mathrm{dR}}{\mathrm{d}N_h}$ is the resolution function.

in another words, we begin with spectrum of true energy and due the resolution we really observe the spectrum of the reconstructed energy. in reference [4] the Figure 2 of this paper have these two distributions. We reproduce here this figure in 8

- Assuming that the near detector is better than the far detector, we can use the same plot to study the tau neutrino flux in this case. We can just use the same plot, but now we set $L = 0$. This gives the number of events due to tau neutrino in our model (the expected number in the SM is zero.)

Appendix B: NOνA and T2K - Epsilon et and mut

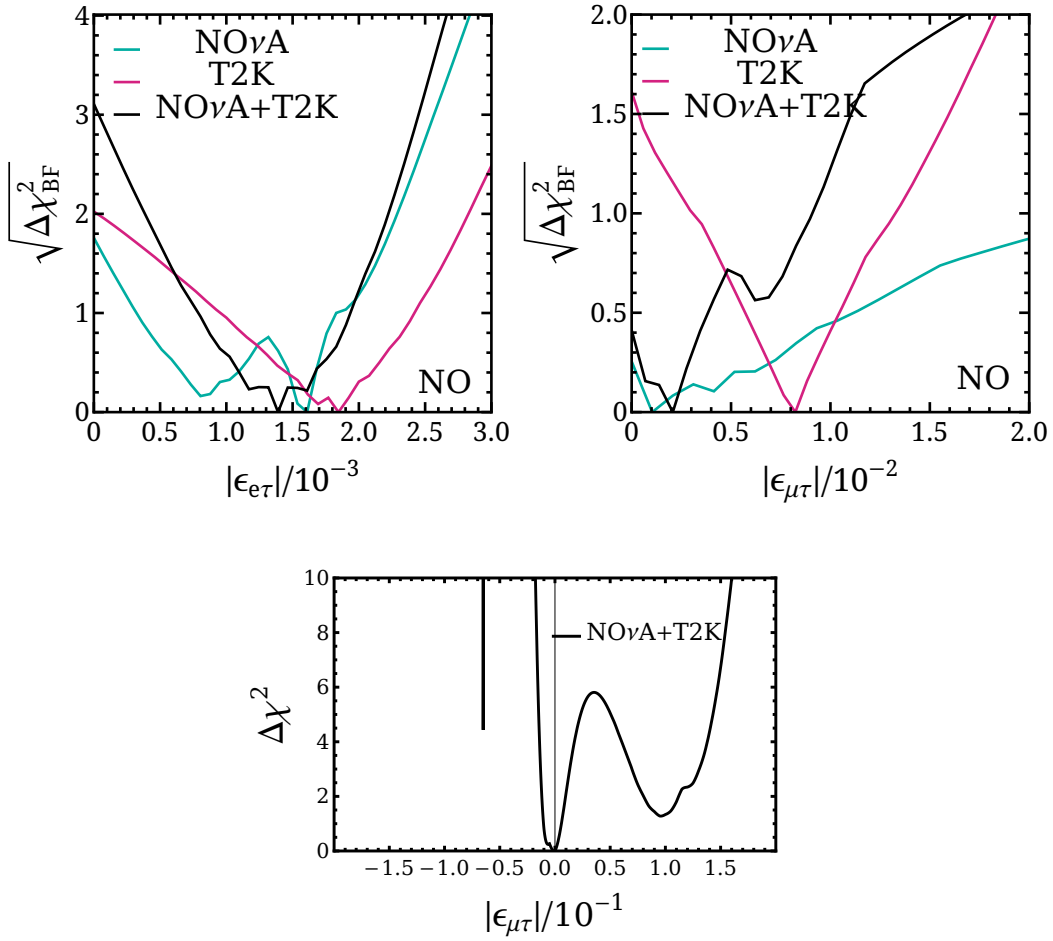

[1] A. Falkowski, M. González-Alonso, and Z. Tabrizi, JHEP **11**, 048 (2020), arXiv:1910.02971 [hep-ph].
[2] A. Falkowski, M. González-Alonso, J. Kopp, Y. Soreq, and Z. Tabrizi, JHEP **10**, 086 (2021), arXiv:2105.12136 [hep-ph].
[3] V. Bresó-Pla, A. Falkowski, M. González-Alonso, and K. Monsálvez-Pozo, JHEP **05**, 074 (2023), arXiv:2301.07036 [hep-ph].
[4] A. De Gouvêa, K. J. Kelly, G. V. Stenico, and P. Pasquini, Phys. Rev. D **100**, 016004 (2019), arXiv:1904.07265 [hep-ph].
[5] C. Giunti, C. W. Kim, J. A. Lee, and U. W. Lee, Phys. Rev. D **48**, 4310 (1993), arXiv:hep-ph/9305276.
[6] E. K. Akhmedov and J. Kopp, JHEP **04**, 008 (2010), [Erratum: JHEP 10, 052 (2013)], arXiv:1001.4815 [hep-ph].
[7] A. Kobach, A. V. Manohar, and J. McGreevy, Phys. Lett. B **783**, 59 (2018), arXiv:1711.07491 [hep-ph].
[8] L. Alvarez-Ruso *et al.* (NuSTEC), Prog. Part. Nucl. Phys. **100**, 1 (2018), arXiv:1706.03621 [hep-ph].
[9] P. Huber, J. Kopp, M. Lindner, M. Rolinec, and W. Winter, Computer Physics Communications **177**, 432–438 (2007).
[10] M. C. Gonzalez-Garcia, M. Maltoni, J. a. P. Pinheiro, and A. M. Serenelli, JHEP **02**, 064 (2024), arXiv:2311.16226 [hep-ph].